The Journal of Undergraduate Research in Physics

CONTENTS

VOLUME 7, NUMBER 2

APRIL 1989

Published by the Physics Department of Guilford College
for
The American Institute of Physics and The Society of Physics Students

THE JOURNAL OF UNDERGRADUATE RESEARCH IN PHYSICS

This journal is devoted to research work done by undergraduate students in physics and its related fields. It is to be a vehicle for the exchange of ideas and information by undergraduate students. Information for students wishing to submit manuscripts for possible inclusion in the Journal follows.

ELIGIBILITY

The author must have performed all work reported in the paper as an undergraduate. The subject matter of the paper is open to any area of pure or applied physics or physics related field.

SPONSORSHIP

Each paper must be sponsored by a full-time faculty member of the department in which the research was done. A letter from the sponsor, certifying that the work was done by the author as an undergraduate and the the sponsor is willing to be acknowledged in the paper, must accompany the manuscript if it is to be considered for publication.

SUBMISSION

Two copies of the manuscript, the letter from the sponsor and a telephone number where the author can be reached should be sent to:

Dr. Rexford E. Adelberger, Editor
THE JOURNAL OF UNDERGRADUATE
RESEARCH IN PHYSICS
Physics Department
Guilford College
Greensboro, NC 27410

FORM

The manuscript should be typed, double spaced, on 8 1/2 x 11 inch sheets. Margins of about 1.5 inches should be left on the top, sides, and bottom of each page. Papers should be limited to fifteen pages of text in addition to an abstract (not to exceed 250 words) and appropriate drawings, pictures, and tables. Manuscripts may be submitted on a disk that can be read by a MacIntosh™. The files must be compatible with MacWrite™ or MicroSoft Word™. Illustrations should be in a MacDraw™ or MacPaint™ PICT format.

ILLUSTRATIONS

Line drawings should be made with black ink on plain white paper. Each figure or table must be on a separate sheet. Photographs must have a high gloss finish.

CAPTIONS

A brief caption should be provided for each illustration or table, but it should not be part of the figure. The captions should be listed together at the end of the manuscript

EQUATIONS

Equations should appear on separate lines, and may be written in black ink.

FOOTNOTES

Footnotes should be typed, double spaced and grouped together in sequence at the end of the manuscript.

SUBSCRIPTION INFORMATION

The Journal is published bianually, with issue one appearing in October and issue two in April of the next year. There are two issues per volume.

TYPE OF SUBSCRIBER	PRICE PER VOLUME
Individual	$US 5.00
Institution	$US 10.00

Foreign subscribers add $US 2.00 for surface postage, $US 10.00 for air freight.

To receive a subscription, send your name, address, and check made out to **The Journal of Undergraduate Research in Physics (JURP)** to the editorial office:

JURP
Physics Department
Guilford College
Greensboro, NC 27410

Back issues may be purchased by sending $US 15.00 per volume to the editorial office.

The *Journal of Undergraduate Research in Physics* is published by the Physics Department of Guilford College for the American Institute of Physics and the Society of Physics. **ISSN 0731-3764**

An Editorial - by Rexford E. Adelberger

MOVING PAINS - THE CONSEQUENCE OF PHYSICISTS MANAGING AN ADMINISTRATIVE CHANGE ... *I knew I should have taken couple of those easy management courses in college.*

Over the past year, the Society of Physics students has been suffering through the administrative changes taking place in the American Institute of Physics. When Kenneth Ford became the CEO of the Institute, he decided to restructure the organization and hired some new people to head the various branches of the organization.

The SPS is part of the Education Division of the Institute. It is a very small part of this large scientific publishing organization. However, it is important to the AIP because it is one of the few parts of the Institute that can be considered non-profit educational, and hence keep the whole organization at the preferred status of 'tax-exempt' in the eyes of the IRS. Since we are part of the education office, the executive office (without an executive officer) of the SPS, along with the rest of the division, moved to the AIP offices in Washington DC.

Physicists have have always felt that one of their skills was to be able to design experiments which clearly could tell the truth about physical reality. I have often heard the story how R. R. Wilson directed the design and construction of the accelerator at Fermi Lab in less than the expected time and came in under budget. I remember remarking to some friends that what we really needed was to have a physicist as President if we wanted to extract ourself from the political mess in which we find ourselves.

At the same time, I remember one of my college math teachers teaching me the power of the counter-example. I suspect that the move of the SPS to Washington DC is a counter-example to the administrative acumen of the director of Fermi Labs. The military has a number of interesting acronyms that describe the transition. Until the last few weeks, it wasn't clear that there was a center-of-mass for the system to which a net force could be applied to accelerate it in the correct direction.

One of the characteristics of a good physicist is that the directions taken in future actions are seldom the same as those that lead to previous mistakes. The folk expression for this is: "we learn from our mistakes". My view from the ivory tower at Guilford College indicates that the system normal is now straightening out. It appears that the SPS is once again acting as an organization that is to support and encourage the physics students in the USA.

The Society has two important programs that help the members of the various chapters either publicize physics or actually take part in a chapter research program. The former are the Marsh A. White awards. These awards were established in honor of an early president of the Society who currently acts as historian for the Society.

The latter are a set of competitive awards for the various chapters to assist in group research projects. Through this program, the Society is trying to get the undergraduate students to try to be physicists, instead of just studying about physics. To me, this is one of the most significant things the SPS can do. These awards are sponsored by the Allied-Signal Corporation. The support given by this program has resulted in a number of papers that have been published in the Journal of Undergraduate Research in Physics.

It is clear to me that this program is working. The students manage to carry projects out, from the initial idea, to creating a detailed proposal, to doing the experiment, to publishing their results so that the rest of the physics community can learn from their experience. I doubt that any textbook centered course can teach this!

This year's Allied-Signal Award committee recently met and funded 4 of the 12 proposals submitted by the various chapters. So that the readers of the

Journal can learn about the successful proposals and perhaps be encouraged to submit proposals of their own in future years, I am publishing the abstracts of the successful proposals.

San Jose State University - **INSTABILITIES OF WATER COLUMNS** - A water column, flowing down a tube, is stopped by a flat horizontal barrier. The water-air interface is smooth for large separation (h) between the tube and the barrier. For h less than a threshold value, h_c, the interface is observed to be unstable and bifurcates into a standing wave. This phenomenon is closely related to the surface tension of the water-air interface. Measurements will be made on the wavelength of the standing waves as a function of h, the flow velocity, and the radius of the tube. The bifurcation is supercritical and is analogous to a second order phase transition. Theoretical analysis will also be done.

University of Missouri-Rolla - **THE SUPERCONDUCTOR SHADED-POLE INDUCTION MOTOR** - We will build a shaded-pole induction motor using a high T_c superconducting rotor to eliminate current power loss in the rotor. For comparison, we will build a normal conducting rotor of the same design for use with the same motor. We will analyze the power efficiencies of the motor using each rotor.

Wesleyan University - **RADIATION DOSIMETRY USING EXOELECTRON EMISSION** - When exposed to ionizing radiation, energetic defects are created within many inorganic materials. Thermal annealing heals the defects and energy is released partly as exoelectronic emission (EE). We propose to study the thermally stimulated EE from thick oxides on silicon as a means of measuring radiation doses.

The University of Wisconsin - Platteville - **LASER DESORPTION OF ISOTOPIC ^{13}CO FROM MOLYBDENUM** - We propose to expose a clean molybdenum foil to isotopic carbon monoxide has (^{13}CO) in a vacuum chamber which has been evacuated to 10^{-10} torr to produce both physically adsorbed and chemically adsorbed ^{13}CO. With the ^{13}CO bonded to the surface, the surface will be irradiated with a laser having a sufficiently energetic photons to desorb the physiosorbed ^{13}CO, but not the chemically adsorbed ^{13}CO. This will be detected by a rise in the chamber pressure. The chemisorbed ^{13}CO, having a bond energy greater than that of the irradiating photons, will then be removed thermally. If the thermal desorption peak of chemisorbed ^{13}CO is unchanged by the laser irradiation, we can conclude that the photons have selectively removed the physiosorbed ^{13}CO. Because a typical clean ultrahigh vacuum system contains a large fraction of mass 28 gases such as N_2 and CO, we believe that using isotopic ^{13}CO will improve the signal to noise ratio for our data.

Northern Arizona University - **SYNTHESIS OF HIGHLY OXIDIZED NICKELATE COMPOUNDS - A POSSIBLE NEW BREED OF HIGH TEMPERATURE SUPERCONDUCTORS** - We plan to develop a new solid state method of synthesizing highly oxidized inorganic compounds. We shall apply this method to the synthesis of Ba-Bi-Ni oxides and Ba-Pb-Ni oxides so that we can study their electrical properties.

Southwestern Oklahoma State University - **PHOTOMETRIC MEASUREMENTS OF TRACE GASES IN THE ATMOSPHERE** - It is proposed to make quantitative measurements of concentrations of ozone and possibly other gases in the stratosphere. This will be accomplished by photometric measurements using a modified Newtonian telescope with controlled intensities of sunlight and spectral filters. Calibration will be provided using gas cells with known gas concentrations.

I guess that the Allied-Signal Awards are a sign that despite the administrative problems, the SPS is alive and functioning. It is still real.

A NUMERICAL SOLUTION TO THE SPRING PENDULUM PROBLEM

B. Benedict and G. Bruner
Department of Physics
The University of Wisconsin-Platteville
Platteville, WI 53818

ABSTRACT

A pendulum consisting of a bob suspended from a spring executes a motion which is a combination of spring like oscillations and pendulum like swings. Since the differential equations of this motion are non-linear, the spring pendulum provides an interesting example of a system that must be treated with numerical methods. Olsson[1] has pointed out that under certain conditions the pendulum will exhibit autoparametric resonance. The differential equations of motion for such a system have been solved numerically and the results compared to that of an actual pendulum in the laboratory. The k/m ratio of the spring pendulum was selected to approximate the value required to observe autoparametric resonance. The results of the numerical solution appear to be in qualitative agreement with the motion observed in the laboratory.

1. M.G. Olsson, Am. J. of Phys. 44, 122, 1976.

INTRODUCTION

There is a good deal of interest in the autoparametric resonant motion of the spring pendulum system such as shown in Figure 1. [1,2,3] The spring pendulum is a good example of a simple system that exhibits a very complex motion. A typical textbook question asks for the equations of motion for this two dimensional system [4].

Ignoring frictional losses in the system and the rotation of the bob, one can obtain the differential equations of motion from the "approximate" Lagrangian. The equations obtained, however, are non-linear and cannot be solved exactly.

Parametric resonance occurs when there is a transfer of energy between the spring like motion and the pendulum like motion of the system. To easily observe parametric resonance, the natural frequencies of the spring (ω_s) and the pendulum (ω_p) should be chosen such that $\omega_s = 2\omega_p$. Falk has done a thoughtful theoretical analysis of the spring pendulum in which he describes recurrent effects in the parametric spring pendulum. He suggests to start the motion with spring-like oscillations and then observe its evolution to pendulum-like motion. We have chosen, however, to start the pendulum with a finite initial angular displacement

THE NUMERICAL SOLUTION [5]

Choosing the gravitational potential energy " zero" at the pivot height, the approximate Lagrangian for this system becomes:

$$L = T - V = \{[T_{vib} + T_{swing}] - [V_{grav} - V_{spring}]\}$$

$$= \left\{\frac{1}{2}\left(\frac{M_{sp}}{3} + M_b\right)(\dot{r}^2 + r^2\dot{\theta}^2)\right\} \qquad (1)$$

$$-\left\{-\left(\frac{1}{2}M_{sp} + M_b\right) g\, r\cos\theta + \frac{1}{2}k\,(r - r_o)^2\right\}$$

Both authors graduated from UW-Platteville. Brian Benedict minored in phnysics and went to UW-Madison to study Chemistry. Gray Bruner left to study optometry at the University of Indiana.

where M_b is the mass of the bob, M_{sp} is the mass of the spring, r is the distance from the pivot point to the center of the bob and r_o the rest length of the hanging spring and bob.

We have assumed the "bob" to be a point mass and that the spring extended from the pivot point to the center of the bob. The center of mass of the spring, assumed to be at its midpoint, accounts for the $1/2\ M_{sp}\ g \cos\theta$ term in the gravitational energy.

The differential equations of motion obtained from this Lagrangian are:

$$\ddot{\theta} = -\frac{2\dot{r}\dot{\theta}}{r} - \frac{\frac{1}{2}M_{sp} + M_b}{\frac{1}{3}M_{sp} + M_b} g \sin\theta \qquad (2)$$

$$\ddot{r} = r\dot{\theta}^2 + \frac{\frac{1}{2}M_{sp} + M_b}{\frac{1}{3}M_{sp} + M_b} g \cos\theta - k\frac{r - r_o}{\frac{1}{3}M_{sp} + M_b} \qquad (3)$$

Due to the $\dot{r}\dot{\theta}$ term in Equation 2, the equations of motion cannot be solved by any simple analytical method. They can, however, be solved numerically. The Galilian equations of motion (Equations 4-7) were used in conjunction with Equations 2 and 3 to obtain approximate values for r, θ and $\dot{\theta}$.

$$r = r_o + \dot{r}\,\Delta t + \frac{1}{2}\ddot{r}\,(\Delta t)^2 \qquad (4)$$

$$\dot{r} = r_o + \ddot{r}\,\Delta t \qquad (5)$$

$$\theta = \theta_o + \dot{\theta}_o\,\Delta t + \frac{1}{2}\ddot{\theta}\,(\Delta t)^2 \qquad (6)$$

$$\dot{\theta} = \dot{\theta}_o + \ddot{\theta}\,\Delta t \qquad (7)$$

Values of $\ddot{\theta}$ and $\ddot{r}$ are obtained from Equations 2 and 3. The initial conditions determined the first pair of values for $\ddot{r}$ and $\ddot{\theta}$. These accelerations and the initial conditions were then used to determine r, $\dot{r}$, θ and $\dot{\theta}$ at $t = \Delta t$. It is crucial that the time interval Δt be sufficiently small (.0001 sec) so that $\ddot{r}$ and $\ddot{\theta}$ could be assumed to be constant over the interval.

New values of $\ddot{r}$ and $\ddot{\theta}$ were then calculated using the r, $\dot{r}$, $\dot{\theta}$, θ values just obtained. Equations 4-7 were then reevaluated to obtain new values of r, $\dot{r}$, θ, $\dot{\theta}$ at $t = 2\Delta t$. This process was coded into a computer and the results fed into a plotter to record the position of the bob through a complete swing.

To closely follow the evolution of the motion, a separate plot was made for each one-way swing. This was done by testing the sign of each value of $\dot{\theta}$. If the sign was opposite to that of the preceeding one, the pendulum had begun a return trip and a new graph started. The predicted motion was then compared to that of a real spring pendulum system.

EXPERIMENTAL

A schematic drawing of the spring pendulum arrangement is shown in Figure 1. The spring used

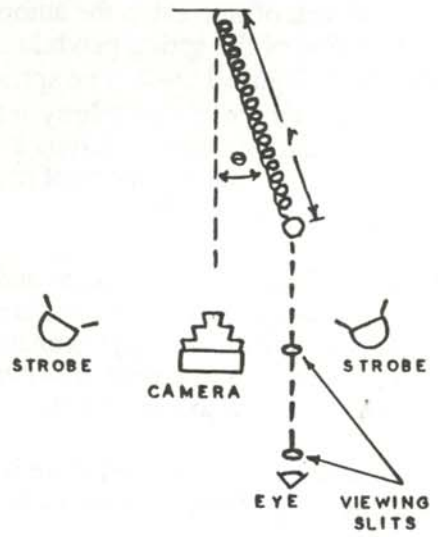

Figure 1

A schematic drawing of the spring pendulum, camera, and strobes

in this experiment had a spring constant (k) of 14.59 N/m, a horizontal rest length of 0.402 m and a mass of 0.186 kg. To observe autoparametric resonance, the mass of the bob was adjusted to 0.219 kg so that the spring of the horizontal rest length l_o was stretched to 4.3 l_o. This special m/k ratio was calculated by Olsson[1] to be one that would result in the autoparametric resonance condition where $\omega_{spring} = 2\ \omega_{pendulum}$.

The path of the bob was recorded with stroboscopic photography. The two synchronized strobe lights (for adequate light) were set at 1250 flashes/minute. The pendulum bob was held in its initial rest position with a thread. Typical initial values for r and θ were 0.88 m and 0.1 radians respectively.

After the system appeared stable, the thread was burned. The camera shutter was opened and closed at the appropriate times to record only the one-way swing desired. Since the initial position of the pendulum was critical, a mark on the bob was viewed through two apertures placed about 2 meters apart to optically align the system. As a check on the reliability of the release, photographs were taken of a given swing several times. These photographs appear to be identical.

RESULTS AND DISCUSSION

Figure 2 shows the photographs of the first sixteen swings of the pendulum. Figure 3 shows the results of the numerical solutions for the same swings. The agreement is quite good, particularly in the first few frames.

The periodic nature of the predicted motion is evident by looking at Figures 3-1 and 3-11. The actual pendulum also exhibited this recurring motions as shown in Figures 2-1 and 2-11.

The energy transfer between the spring-like and the pendulum-like motion is not complete, but clearly evident in Figures 2-11 and 2-16.

The appropriate frequency for the two modes of oscillation is also visible. For each swing of the pendulum (one-half period), the spring oscillation goes through one complete cycle.

The agreement between Figures 2 and 3 is qualitatively very good despite the simple model of Equation 1. The real spring did not extend from the pivot point to the center of the bob. The straightened portions of the spring on either end amounted to a total of about 6 cm. When these corrections were inserted into Equation 1, no appreciable difference was found in the numerical solution

The model also ignored the kinetic energy of rotation about the center of mass of the bob. This energy was small compared to that of either mode of oscillation.

A noticeable quantitative difference between the numerical solution and the actual motion appears in the amplitudes of the motion. The most spring-like oscillations appear in Figures 3-1 and 3-11 with equal amplitude, while the corresponding real motion (Figures 2-1 and 2-11) show the amplitude decreasing by 4%. An even greater discrepancy appears in the pendulum like motion. The theoretical model (Figures 3-6 and 3-16) show equal amplitudes which the real motion (Figures 2-6 and 2-16) show a decrease of 14%. This loss in amplitude was traced to the pendulum support which was more susceptible to horizontal motion than vertical motion.

CONCLUSION

The numerical method used was shown to be adequate for solving Equations 2 and 3 provided a sufficiently small time interval was used. The agreement between Figures 2 and 3 demonstrate this.

While this project was pedagogically motivated, the results are of interest in the study of other physical systems. A molecule which is chemically bound to a surface can be thought of as a spring pendulum, executing a motions which is a combination of swinging and stretching modes of vibration. As Falk[3] points outs, this models "was suggested by Fermi to explain the equipartition of energy in a system of almost linear oscillators" such as a solid crystal.

ACKNOWLEDGMENTS

The authors wish to thank Janice Abraham for help in preparing the manuscript and Bernie Cook for his help in providing the experimental apparatus. We thank Dr. Glen Brooks and his students for their contribution to the photographs and Rosemary

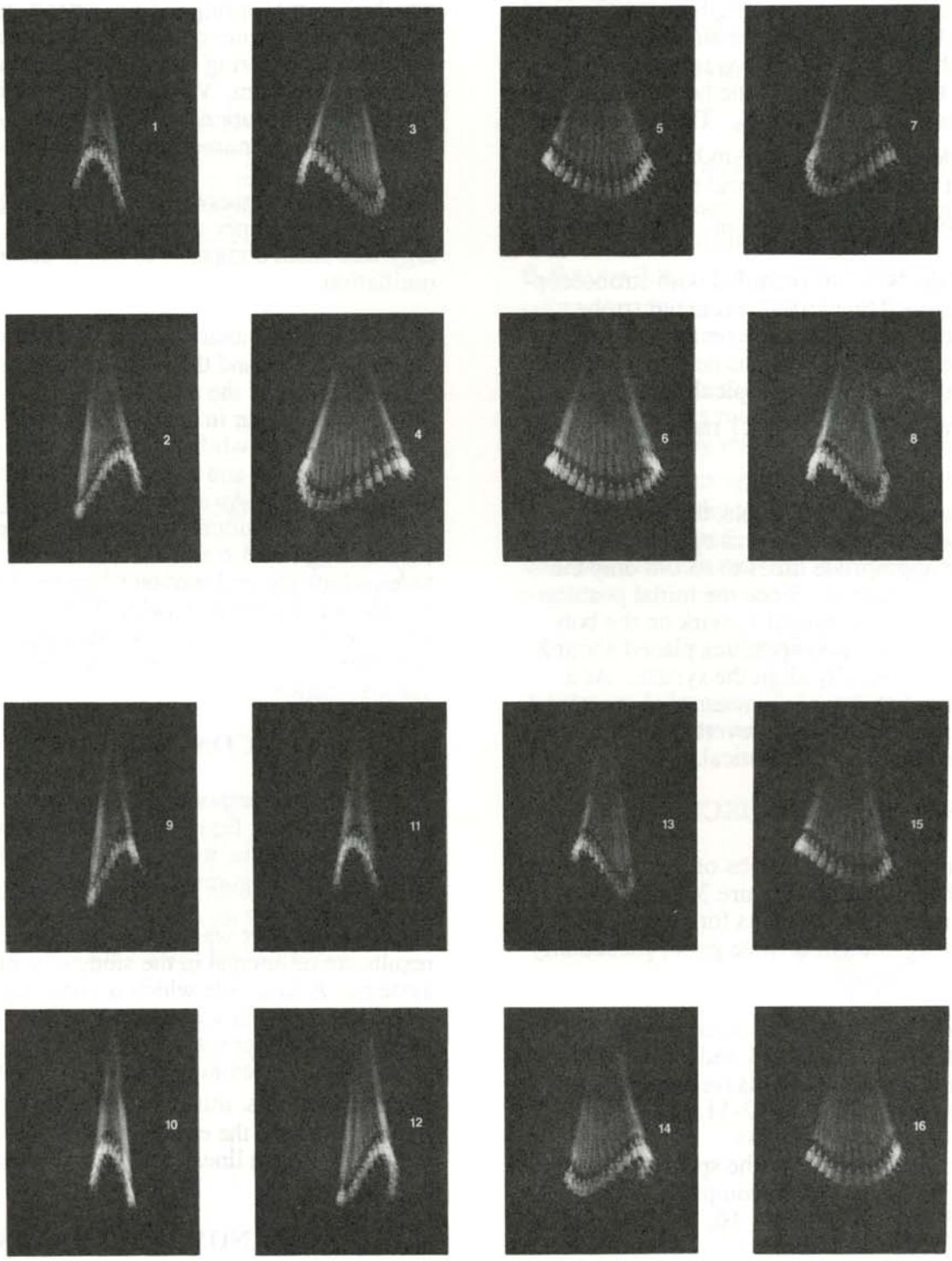

Figure 2
Stroboscopic photographs of the first sixteen complete swings of the pendulum. Each frame shows a one-way swing of the pendulum and can be compared to the corresponding swing drawn by the computer in Figure 3.

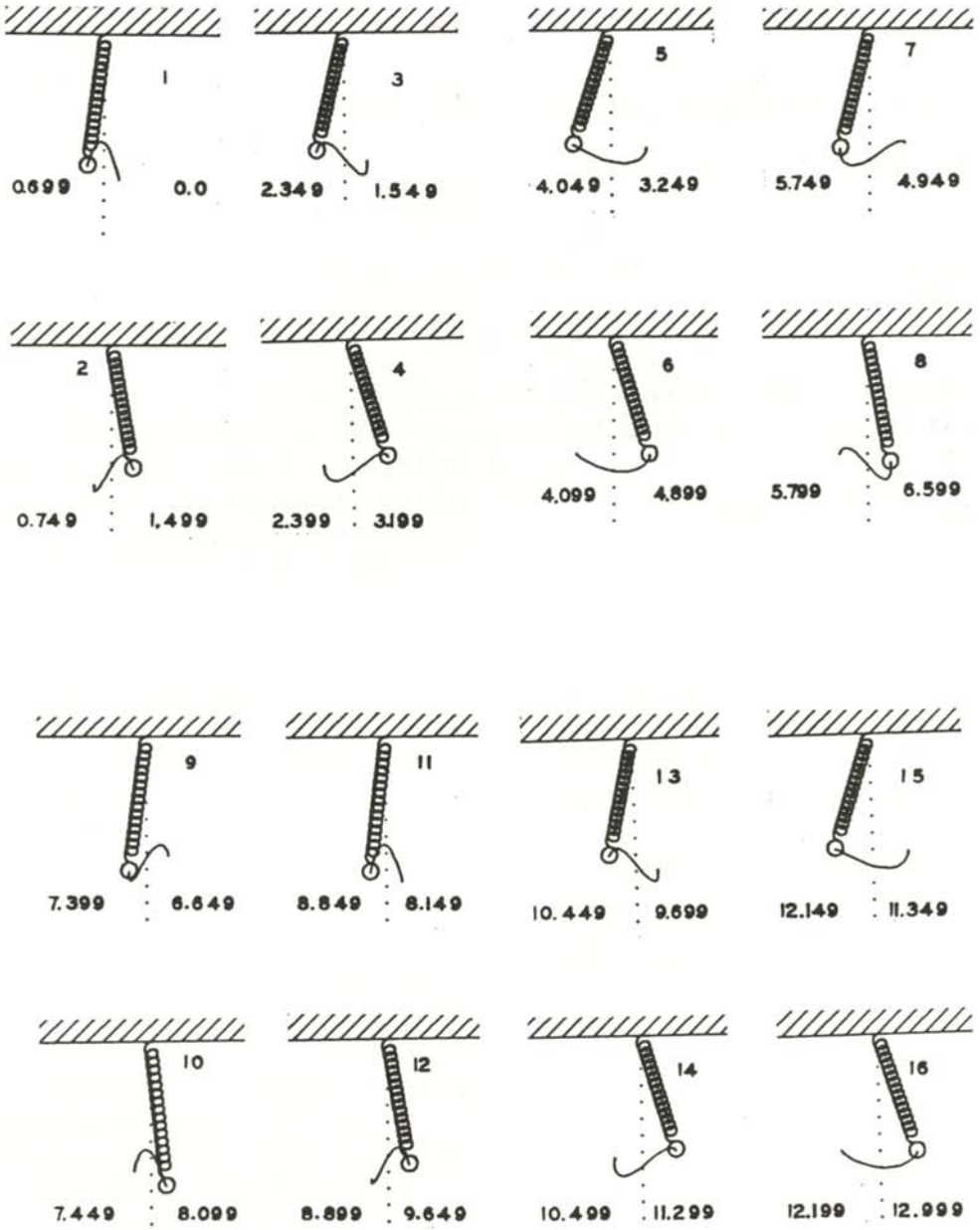

Figure 3

Computer drawings of the first sixteen swings as found from Equations 2-7. The numbers in the lower corners of each frame are the times at which the bob was at that particular position (in seconds)

Legler for her assistance in the laboratory.

REFERENCES

1. M.G. Olsson, Am. J. of Phys., 44, 1211, 1976.

2. T.E. Cayton, Am. J. of Phys. 45, 723, 1977.

3. L. Falk, Am. J. of Phys., 46, 1120, 1978.

4. V. Barger and M. Olsson, Classical Mechanics: A Modern Perspective, McGraw Hill, New York, 1973, p. 80.

5. The swinging pendulum is frequently chosen to exemplify a particular analytical technique. See for example, a. H. Nayfeh, Peturbation Metods, Wiley, New York, 1973.

FACULTY SPONSOR

Dr. Fred Domann
Department of Physics
University of Wisconsin - Platteville
Platteville, WI 53818-3099

RESTRICTED VALENCE PERCOLATION AS A MODEL FOR FRACTALLY ROUGH SILICATE PARTICLES

Lawrence Gates
Department of Physics
Dalhousie University
Halifax, Nova Scotia, Canada B3H 3J5

ABSTRACT

In this computer simulation, restricted valence percolation is used to construct fractally rough structures. We compare this simulation with a poisoned Eden growth model, which in a recent letter by Keefer and Schaefer[1], has been proposed to describe the process by which fractally rough silica colloids may form.

1. K.D. Keefer and D.W. Shaefer, Phys. Rev. Lett. 56, 2376, 1986.

BACKGROUND

Surface fractals are particles whose surface area grows as a function of the cluster's radius, raised to some some power d_s .

$$S \alpha R^{d_s} \qquad (1)$$

where S is the surface area and R the cluster radius. Using small angle X-ray scattering, Keefer and Schaefer[1] were able to find the surface fractals of silica particles in solution. These silicate particles, grown in partially hydrolyzed silicon tetraethoxide [$Si(OC_2H_5)_4$, TEOS], may form fractal structures in which restricted valence percolation[2] can be sufficient to describe the physical system. A paper by De'Bell and Jan[3] indicates that although both restricted valence and poisoned Eden growth models may produce the same structures, the fractal dimension of restricted valence percolation clusters, very close to the percolation threshold[4], will describe the growth of rough silica colloids without requiring a new theoretical model.

In ordinary percolation modeling, the lattice sites are filled with either a 0 or a 4 valence. The computer assigns the 4 valence with probability p. The mean cluster size is defined as:

$$M(p) = \frac{\sum_i S_i^2}{\text{system size}} \qquad (2)$$

where S_i is the number of sites in cluster i and p is the probability of a valence 4 being assigned to a site.

The percolation threshold, p_c, is the probability at which one finds a cluster which spans the lattice. Close to the percolation threshold, the mean cluster size is expected to diverge according to:

$$M(p) \alpha | p_c - p |^{-\gamma} \qquad (3)$$

Lawrence is a fourth year honours physics student at Dalhousie University and worked there on an NSERC grant during the summer of 1987. He is interested in studying nuclear physics in graduate school.

where p is the probability of 4-valence sites, p_c the percolation threshold and γ is the critical exponent.

The fractal dimension[4] d_f is defined for a cluster grown at threshold by:

$$S(l) \alpha l^{d_f} \qquad (4)$$

where S(l) is the number of sites in the cluster and l is the lattice size. Taking the natural log of equation 4 yields:

$$\ln [S(l)] = d_f \ln [l] + C \qquad (5)$$

where C is a constant. The fractal dimension can be found by measuring the slope of a plot of the natural log of S(l) vs the natural log of l.

The Simulation

In the simulations reported here, an n x n square lattice was constructed where each lattice site had a valence associated with it ranging from 0 to 4. The computer assigned a value to each site. If a specific site has a valence of 4, it can connect with each of its 4 neighboring sites provided the neighboring site has a valence greater than 0. When 2 sites become connected in this way, their respective valences are decreased by one. Each site is analyzed in this way by the computer until no more connections are possible.

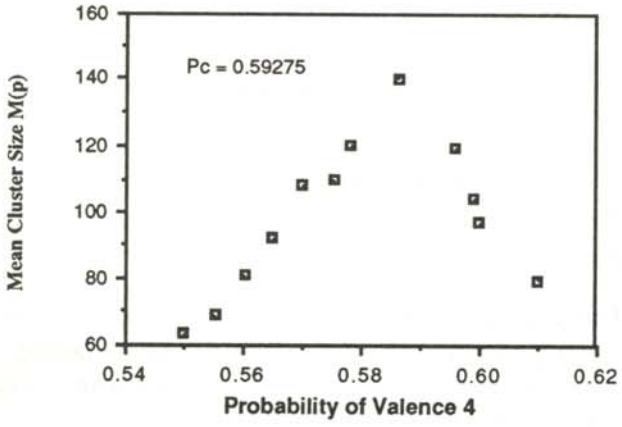

Figure 1
Mean cluster size vs. percolation probability for an N = 100

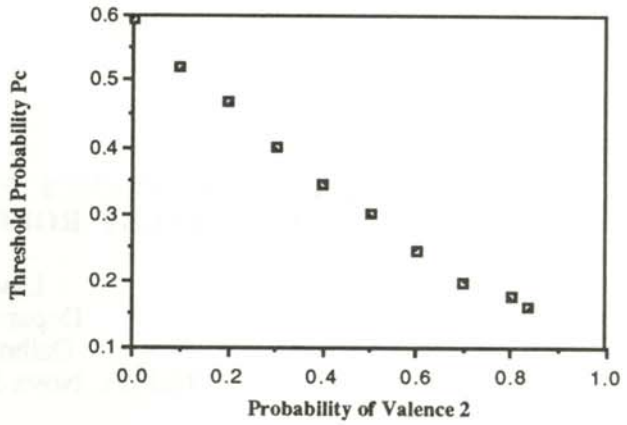

Figure 2
Percolation threshold vs. 2-valence probability for an N = 100 size lattice.

When individual sites are connected to their neighbors, they form part of a cluster. The clusters usually contain many connected sites and can grow to span the entire system.

Restricted valence percolation is when sites can have valences other than 4. In our restricted valence percolation model, we assign sites with valence 2 with a probability X. Ordinary percolation then would be restricted valence percolation with X=0.

RESULTS

Figure 1 shows the mean cluster size of an ordinary percolation model as a function of the probability p of a site having a valence of 4. . Examination of Figure 1 shows the threshold probability, p_c, for percolation.

As X, the probability of a site having valence 2, increases, p_c decreases until there are no sites with 0 valence. Figure 2, our simulation for an N = 100 lattice size, shows this effect.

Figure 3 is plot of ln[S(l)] vs. ln[l] for a cluster grown at $p_c = 0.59275$ and X = 0 for an N = 200 size lattice. The slope of this line is the fractal dimension for these particular circumstances. We ran simulations for X = 0, X = 0.3 and X = 0.83587. X = 0.83587 is the maximum 2-valence probability that gives a percolation cluster. We found that d_f was consistent with the result:

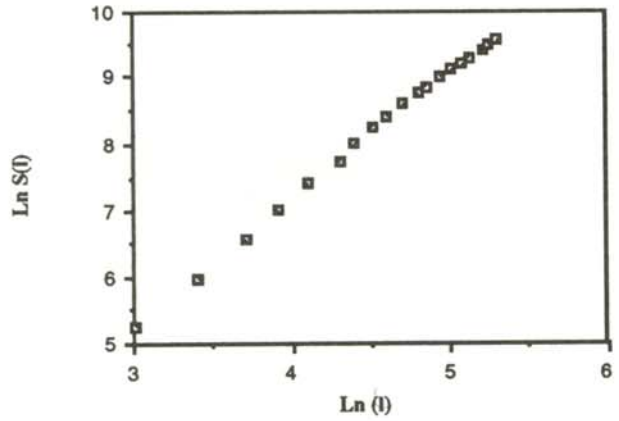

Figure 3
Ln[S(l)] vs. ln[l] for a cluster grown at $P_C = 0.59275$ and X = 0 for an N=200 size latice.

$$d_f = 1.92 \pm 0.03 \qquad (6)$$

in each case. This indicates that the fractal dimension does not change as X increases. The fractal dimension for ordinary percolation is widely believed to be exactly 91/48 [4]. It appears that the fractal dimension does not change for different values of X if the cluster is grown at the percolation threshold.

CONCLUSIONS

It is suggested that restricted valence percolation can describe the formation of fractally rough colloids such as those grown by Keefer and Schaefer.[1] In particular, if the solution provided threshold conditions in which silicate species could form, the fractal dimension, d_f, would be observed.

REFERENCES

1. K.D. Keefer and D.W. Shaefer, Phys Rev. Lett., 56, 2376, 1986.

2. J. Kertesz, B.K. Chakrabarti and J.A.M.S. Duarte, J. Phys. A., 15, L 13, 1982.

3. K. De'Bell and Naeem Jan, Phys. Rev. Lett., 58, 1154, 1987.

4. D. Stauffer, On Growth and Form, Eds. H.E. Scanley and N. Ostrowsky, Martinus-Nijhoff, 1986.

FACULTY SPONSOR

Dr. K. De'Bell
Department of Physics
Memorial University of Newfoundland
St. John's, Newfoundland
Canada A1B 3X7

A COMPUTER SIMULATION OF THE GEOMETRICAL APPEARANCE OF LARGE OBJECTS AT RELATIVISTIC SPEEDS IN THREE DIMENSIONS

Anthony P. Lyons
Physics Department
Henderson State University
Arkadelphia, AR 71923

ABSTRACT

For almost sixty years after the statement of Einstein's famous theory of special relativity, physicists still assumed that the predicted Lorentz contraction could be photographed by a single observer. This paper deals with a computer simulation of the appearance of geometrical objects moving at relativistic speeds with respect to a single observer. The objects are two-dimensional projections of three-dimensional functions drawn after the transformation equations are used to determine their appearance. To verify the apparent distortion, the mathematical transformations were used to provide a point of view unattainable by an actual observer.

COMPARISON OF LORENTZ CONTRACTION AND GEOMETRICAL APPEARANCE

The Lorentz transformation equations:

$$x' = \gamma (x - vt) \qquad (1)$$
$$y' = y$$
$$z' = z$$
$$t' = \gamma (t - vx/c^2),$$

where $\gamma = 1/\{1 - v^2/c^2\}^{.5}$, can be found in almost any textbook dealing with special relativity. The corresponding axes of the reference frames are parallel. The times t and t' are chosen such that both are zero when the origins of the two coordinate systems coincide.

The transformation equations shown in Equation (1) assume that the object is viewed by a 'Lorentz observer', a whole set of observers, spread throughout the reference frame with synchronized clocks. The observers all simultaneously observe the point (x', y', z') moving in the +x directions at the point (x, y, z) in their reference frame. Since the distances perpendicular to the motion are unchanged, the length (L) along the x axis in the observers reference frame is given by:

$$L = (x_2 - x_1) = (x_2' - x_1')/\gamma = L_o(1 - v^2/c^2)^{.5} \qquad (2)$$

This is the equation of the well known Lorentz contraction.

A real observer, however, is not a Lorentz observer. A real observer is at one point in the rest frame. The observer can be thought of as a camera in the rest frame. To the camera, the alteration of appearance will be more than a simple Lorentz contraction. The light from the extended object reaching the camera at a particular instant comes from different points on the object at different times. There are two reasons for this effect: the Lorentz transformations of Equations (1) and that it takes different amounts of time for the light from different points on the object to reach the camera. Since the object is moving, the camera sees the location of different parts of the object at different times in the camera's frame. This effect is caused by the finite speed of light and is apparent only at relativistic speeds.

Tony is a senior physics major from Nashville, Arkansas. He plans to enter the graduate program in physical oceanography at Texas A&M University.

TRANSFORMATION EQUATIONS FOR A REAL OBSERVER

Transformation equations, consistent with the Lorentz transformation, which account for this effect can be derived as follows. The camera is at rest in its coordinate system on the z axis a distance d from the origin. The extended object's coordinate system is moving perpendicular to the z axis in the +x direction. When $t = t' = 0$, the two origins, 0 and 0', are coincident. For 0' to appear at 0, the instant of observation is $t = d/c$. The light from 0' is emitted at $t = 0$. The light from any other point (x',y',z') in the object's reference frame which appears at the point of the camera must have been emitted at time:

$$t = -\{(x^2 + y^2 + [z-d]^2)^{.5} - d\}/c \qquad (3)$$

The transformation equations which take into account this time lag are: [1]

$$\begin{aligned} x &= (x' + \gamma\beta d) \\ &\quad - \beta\,[(x' + \beta\gamma d)^2 + y^2 + (z' - d)^2]^{.5} \\ y &= y' \\ z &= z' \end{aligned} \qquad (4)$$

where $\beta = v/c$. Using these equations, we can calculate the apparent location of each point on a moving object and create a perspective drawing representing the geometrical appearance of objects moving at relativistic speeds from any desired point of view.

RESULTS

The appearance of several three-dimensional functions (objects) was calculated using the transformations given in Equations (4). The calculations were done in BASIC [2] on a computer equipped with DECRegis [3] graphics. To add realism to the display, perspective drawings [4] were created.

Figures 1 - 3 depict an empty co-ordinate system in two dimensions, view by an observer who is two units from the system. Figure 1 shows the appearance of the coordinate system to an observer at rest. Figure 2 shows the appearance of the same coordinate system moving in the -x direction at $\beta = .6$ and Figure 3 shows the appearance of the same coordinate system moving in the -x direction at $\beta = .95$.

The next three figures depict the function:

$$Z = 2\{\cos(\pi x/L)^5 \ \sin(2\pi y/L)\}$$

at several different velocities. The observer is positioned 10 units above the plane of the page. In Figure 4, the function is at rest with respect to the observer. Figure 5 shows the same function, moving in the -x direction at $\beta = .6$. Notice the appar-

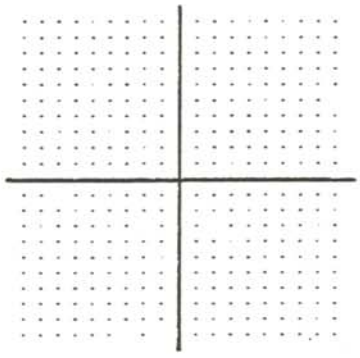

Figure 1
An empty coordinate system at rest with respect top an observer who is two units from the system

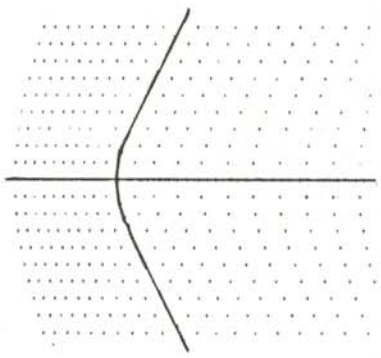

Figure 2
The same coordinate system as in Figure 1, moving in the -x direction at $\beta = .6$

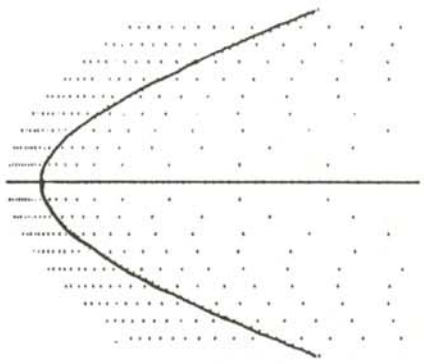

Figure 3
The same coordinate system as in Figure 1, moving in the - x direction at $\beta = .95$.

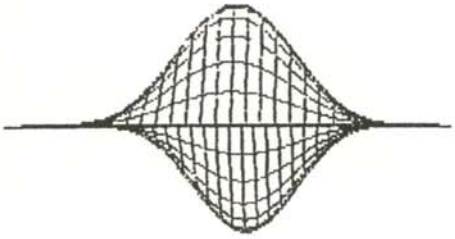

Figure 4
The function, $Z=2\{\cos(\pi x/L)^5\sin(2\pi y/L)\}$, which is at rest with respect to the observer. The observer is positioned above the plane of the page ten units.

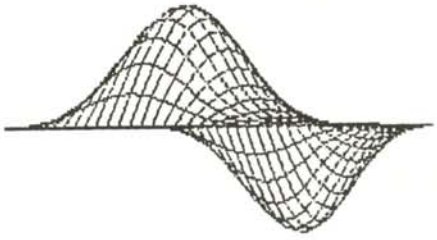

Figure 5
The same function as in Figure 4, moving n the - x direction at $\beta = .6$. Notice the apparent rotation of the function

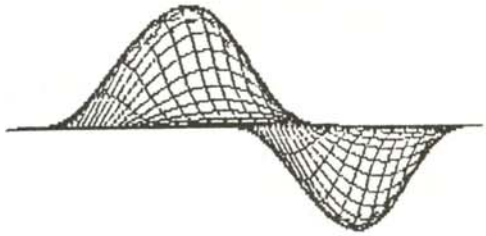

Figure 6
The same function as in Figure 4, moving in the - x direction at $\beta = .95$.

ent rotation of the function. Figure 6 is the same function, now moving in the -x direction with $\beta = .95$.

The last three figures are drawn to represent a viewpoint that cannot be attained by an actual observer, but that help to verify the apparent distortion seen by an observer. The observer is positioned at the top of the page. Figures 7 - 9 show that for an observer who is at one point in the rest frame, in contrast to a 'Lorentz observer' who is spread throughout the rest frame, the apparent distortion is noticeably different from the simple rotation described by Marion. [5]

REFERENCES

1) G.D. Scott and M.R. Viner, Am. J. of Phys., 33, 536, 1965.

2) A listing of this program is available by writing to: Dr. Charles W. Leming, Physics Department, Henderson State University, Arkadelphia, AR 71923.

3) A registered trademark of Digital Equipment Corporation, Maynard, MA.

4) C.W. Leming, Computer Problems for Classical Dynamics, Harcourt, Brace, Jovanovich, New York, 1988, pp. 17-19.

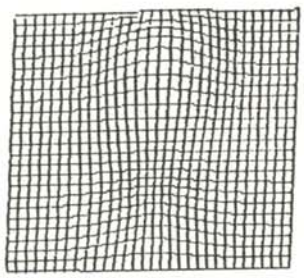

Figure 7
An unattainable view of Figure 4, where the observer is now positioned at the top of the page.

Figure 8
Same view as in Figure 7, but the motion is to the left at $\beta = .6$

Figure 9
Same view as in Figure 7, but the motion is to the left at $\beta = .95$

5) J.B. Marion, Classical Dynamics of Particles and Systems, Academic Press, Inc., Orlando, 1970, pp. 325-326.

FACULTY SPONSOR

Dr. Charles W. Leming
Physics Department
Henderson State University
Arkadelphia, AR 71923

THE CALIBRATION OF A CHARCOAL CANISTER FOR DETERMINATION OF RADON CONCENTRATION

Brett Houser
Department of Chemistry and Physics
Western Carolina University
Cullowhee, NC 28723

ABSTRACT

The use of a charcoal canister is a convenient means of sampling radon concentration in an indoor environment. The canister is calibrated by exposing it to a known concentration of radon gas. The concentration of radon gas was determined by a calibrated Lucas cell. The gamma count rate of the exposed canister is determined by appropriate counting techniques. The calibration curve for the charcoal canister is obtained from the ratio of the gamma count rate and the concentration determined by the Lucas cell.

INTRODUCTION

Measuring radon (Rn^{222}) concentration in an indoor environment has become increasingly important in light of recent links between radon levels and lung cancer [1]. One cost-effective way of making this measurement is with a diffusion barrier charcoal adsorption (DBCA) canister.[2] To make radon concentration measurements with a DBCA canister, it must be calibrated. The calibration relationship is a plot of the radon exposure of the canister to the net gamma counts produced by the exposed canister. The radon exposure is the product of the radon concentration and the canister exposure time.

THE EQUIPMENT

The DBCA is a metal can about 2.5 cm high and 7.0 cm in diameter that contains about 25 gm of activated charcoal which is held in place by a screen of fine wire mesh. This charcoal has a high affinity for gas and will adsorb radon readily. The canister has a snug fitting lid with a 2.0 cm hole in the center which is covered by a bag of desiccant.

The radon concentration was measured with a Lucas cell. A Lucas cell is a metal hemisphere used to take air samples. Samples are taken by first evacuating the cell and then admitting some air of the environment to be tested. The cell is lined with a scintillating material and has a quartz window. Once an air sample has been taken, the Lucas cell is analyzed in a light tight cylinder which contains a photomultiplier tube. This photomultiplier tube is connected through an amplifier to a scaler which counts the light flashes over a set time interval. This Lucas cell was previously calibrated for radon concentration measurements.[3]

The gamma spectroscopy system consists of a 2 in x 2 in sodium-iodide crystal attached to a photomultiplier tube with a built-in preamplifier. The photomultiplier tube is connected to a microcomputer with a multichannel analyzer card.

The radon exposure chamber was a 2.4 l glass desiccant type jar. Radon is a decay product of the uranium series, so uranium ore was used as the radon source in the chamber. The Lucas cell was

---

Brett graduated from Western Carolina University with a physics degree in 1988 and is now working in the radon measurment industry

connected to the chamber via a glass tube. The difficulty with this type of chamber is that there is a continuous build-up of radon instead of a constant concentration of radon.

One way to compensate for this difficulty is to model the radon build-up with a mathematical expression which takes into account the radon build-up in the chamber as well as the radon lost to the charcoal and to nuclear decay. The time rate of change of the number of radon atoms, N(t), is:

$$\frac{dN(t)}{dt} = E\,A_{Ra} - \lambda_{Rn}\,N(t) - \frac{v\,N(t)\,e^{-\frac{t}{t_c}}}{V\,t_c} \qquad (1)$$

where A_{Ra} is the activity of the radium which decays into radon, E is the emanation coefficient which gives the fraction of the radon that escapes the ore sample, λ_{Rn} is the decay constant of the radon, v is the effective adsorption volume of the canister, V is the volume of the radon chamber and t_c is the time constant of the canister. The first term represents the source of the radon. The second term represents the decay of the radon. The third term describes the effect of the canister on the chamber.[4]

Before Equation 1 can be solved, a value for $E\,A_{Ra}$ has to be determined. This is done experimentally by measuring the radon concentration in the chamber after 72 hours of radon build-up without the canister. Without the canister in the chamber, the value of the third term is 0 and the value of the second term is known.

Equation 1 was solved by iterating successive values of time using the relationship:

$$\Delta N = \left\{ E\,A_{Ra} - \lambda_{Rn}\,N(t) - \frac{v\,N(t)\,e^{-\frac{t}{t_c}}}{V\,t_c} \right\} \Delta t \qquad (2)$$

A computer program was used to do this iteration and produced values of average and instantaneous radon concentrations. The ratio of the average to instantaneous radon concentrations is used as a correction factor in calculating the values of radon exposure.

$$\text{Correction factor} = \frac{\text{Average Rn concentration}}{\text{Instantaneous Rn Concentration}} \qquad (3)$$

CALIBRATION METHOD

A standard method for calibrating a DBCA canister is to place a known activity of radium in the canister, seal it, and wait thirty days for secular equilibrium between the radium, radon, and their decay products.[5] The calibration factor of the detectors is derived by integrating the gammas between 270 and 720 keV. With this calibration factor, one can determine the unknown radon concentration from an exposed canister by comparison of gamma counts of the known canister.

The method of calibration of this project is somewhat different. The range of the gamma spectrum used is 0 - 790 keV. The background gamma spectrum is subtracted to produce a net gamma spectrum. The net gamma spectrum is integrated to give the net gamma counts. The net gamma count is then compared to the value of the radon concentration from the Lucas cell. Because there is a continuous build-up of radon in the test chamber, simulations of different radon exposures can be done by varying the time of canister exposure.

THE PROCEDURE

The canister is baked overnight in an oven at approximately 100 C to drive off any radon or water in the charcoal. After the canister is removed from the oven, the hole in the top of the canister is sealed with aluminum tape. The background gamma spectrum is then counted. The hole in the top of the canister is uncovered and the canister placed in the test chamber with the Lucas cell. This time is denoted as t_1. After a specified time, t_2, an air sample is taken and the canister is removed from the test chamber and the hole resealed.

Both the Lucas cell and the canister are allowed to sit for 4 hours so that the radon daughters will be in equilibrium with the radon. This step is useful because it simplifies the calculations of the activities of the daughters in the decay scheme of the radon series. Four hours after t_2, the rate of change of the number of radon atoms, or radon daughters, can be found by the nuclear decay equation for radon.

At time t_3, at least four hours after t_2, the canister and the Lucas cell are analyzed. The time of analysis for the canister and the Lucas cell are 30 minutes and 10 hours respectively. Analysis ending

time is denoted by t_4.

The number of alpha particles detected is divided by the counting interval to give the count rate R(t). The count rates are averaged over the 10 hour interval. This average is corrected back to the rate at time t_3 by:

$$R(t_3) = \frac{\bar{R}(t)\,\lambda_{Rn}(t_4 - t_3)}{1 - e^{-\lambda_{Rn}(t_4 - t_3)}} \qquad (4)$$

This correction is necessary because some decay takes place during the counting interval. The count rate is then multiplied by the efficiency factor for the Lucas cell to give the radon concentration $C(t_3)$. The radon concentration at time t_3 is then corrected to the value at time t_2:

$$C(t_2) = \frac{C(t_3)}{e^{-\lambda_{Rn}(t_3 - t_2)}} \qquad (5)$$

This value is converted to the average radon concentration for the time interval $t_2 - t_1$ by multiplication of the correction factor given by Equation 3. Finally, the average radon concentration is multiplied by the time interval to give the value of the radon exposure.

The data from the exposed canister are corrected in the following manner. The net counts are obtained for the particular canister exposure time. This value is divided by the analysis time to give a count rate. Averaging over the analysis time only changes the value by 0.2%, so this step is ignored. The canister count rate is corrected back to time t_2 in the same manner as seen in Equation 5. This is the value of the corrected net canister count rate.

RESULTS

Canister exposure tests were made for the time periods shown in Table 1. These time periods represent a geometric progression. Normally a DBCA canister would be tested for periods between 4 and 7 days, but because of the build-up of radon concentration in the exposure chamber, shorter time periods could be used.

The calibration curve (Figure 1) is a plot of canister counts versus radon exposure. The error bars for

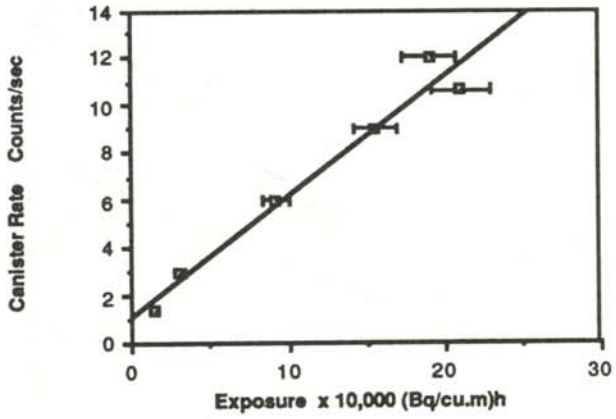

Figure 1
A plot of the calibration curve. Canister count rate is on the vertical axis and radon exposure on the horizontal axis.

the radon exposure correspond to a 9% uncertainty in the calibration factor of the Lucas cell. [3] The error bars for the count rate of the canister are too small to plot. The line shown:

$$\text{Radon Exposure} = \frac{\text{Canister Count Rate} - 1.05}{5.25 \times 10^{-5}} \qquad (6)$$

is the regression line determined by a least squares fit. The correlation coefficient of 0.971 suggests that the linear model is appropriate for this data.

DISCUSSION OF INTEGRATION TECHNIQUES

The calibration curve is based on the integration of the corrected gamma spectrum from 0 - 790 kev. There is some question of the appropriateness of

Canister exposure hr	Exposure (Bq/m^3)h	Count Rate sec^{-1}
5	15200	1.43
10	31300	2.81
30	93700	6.10
45	157000	8.98
54	162000	10.1
72	191000	12.1
72	214000	10.6

Table 1
Data for the calibration curve.

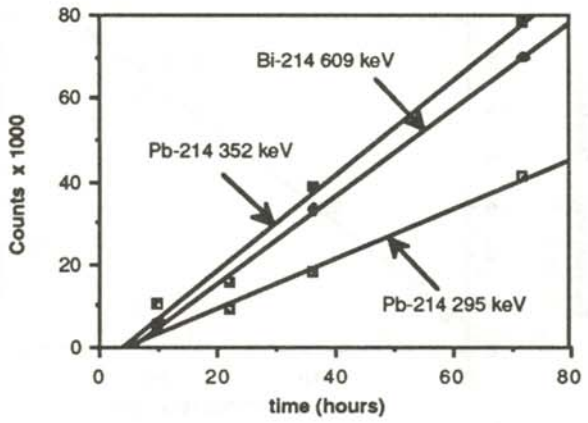

Figure 2

A plot of gamma counts versus time for the Pb^{214} peak at 295 keV and 352 keV and Bi^{214} at 609 keV.

this integration range for the calibration curve. The alternative to summing up the entire range is to integrate the counts under a peak. There are three peaks that are suitable for integration, those for Pb^{214} at 295 keV, Pb^{214} at 352 keV and Bi^{214} at 609 keV. To determine the best calibration curve, one based on the integration of a single peak or one based on summing the entire spectrum, one plots counts under the peak versus canister exposure time and looks for the graph with the 'smoothest' features.

Tests were run to determine the integrated counts for exposure times of 10, 22, 36 and 72 hours. The counts in a peak were determined by a software package that fitted each peak to a Gaussian curve. Figure 2 shows a very smooth relationship between counts and time for all three peaks. Figure 3 indicates that the sum of the entire spectrum also produces a very smooth curve. This suggests that there is no significant difference between the use of integrated peaks and the sum of the spectrum in the calibration curve.

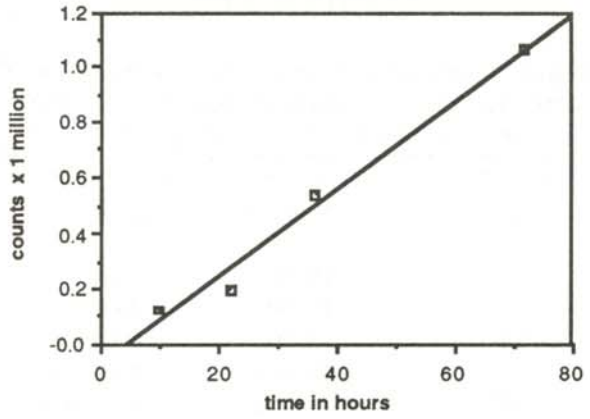

Figure 3

A plot of the sum of the total gamma spectrum as a function of time.

CONCLUSIONS

This project developed and tested a method for calibration of a charcoal canister for measurement of radon concentrations. The method of calibration uses a convenient sum of counts from the spectrum, does not require a constant radon concentration or an expensive radon exposure chamber, and can be done with counting equipment commonly found in radioisotope labs.

ACKNOWLEDGMENTS

The author would like to thank Dr. Glenn Liming for his time and assistance. His support made this research and subsequent paper possible.

REFERENCES

1) C.T. Hess, "Environmental Radon and Cancer Correlation in Maine", Health Physics 45, 1983, pp 339-348.

2) B.L. Cohen and R. Nason, "A Diffusion Barrier Charcoal Adsorption Collector for Measuring Rn Concentrations In Indoor Air", Health Physics 50, 1986, pp. 457-463.

3) The efficiency factor for the Lucas cell is 127±12 (pCi/l)/(counts/sec).

4) B.L. Cohen and R. Nason,"Radon Chamber for Calibration of Charcoal Detectors", Health Physics 51, 1986, pp 135-137.

5) EERF Standard Operating Procedures For Radon^{222} Measurements Using Charcoal Canisters, February 1987.

FACULTY SPONSOR

Dr. Glenn Liming
Department of Chemistry and Physics
Western Carolina University
Cullowhee, NC 28723

THE SPEED OF CARBON DIOXIDE BUBBLES RISING IN A GLASS OF BEER

William DeZarn and Mark Ward
Physics Department
Guilford College
Greensboro, NC 27410

ABSTRACT

We used a video camera to record the motion of bubbles rising in a glass of beer. A video recorder, with freeze frame and single frame advance features, was used to collect the distance-time information on the motion of a single bubble. The experimental data showed the bubbles rising through the beer at a constant speed of $(1.5 \pm .1) \times 10^{-1}$ m/sec. A computational analysis of the motion was done. From this analysis, we deduced that the radius of the bubbles had a constant value of 3.3×10^{-5} m. Our data showed that a bubble rising through beer is not a simple thermodynamic process.

INTRODUCTION

In beer, as in all carbonated drinks, carbonic acid is dissolved in the liquid. The carbonic acid contains carbon dioxide that is held in equilibrium by the presure of the surroundings. When the pressure of the surroundings is decreased below the vapor pressure of the carbon dioxide, the gas is released out of the liquid and bubbles are formed. The bubbles form at nucleation sites in the liquid and on the surface of the container. After their formation, the bouyant force causes them to float upward through the liquid.

As the bubbles float upward through the liquid, the pressure exerted on them by the fluid decreases. If the gas in the bubble obeys some simple thermodynamic rule, such as isothermal or adiabatic behavior, the volume of the bubble should increase as it rises through the beer. Larger bubbles should rise faster than small ones, so the bubbles should accelerate upwards.[1]

EXPERIMENTAL DESIGN

A video camera, a video cassete recorder, a slide projector, a meter stick and a clear plastic container of a carbonated liquid were used to obtain our experimental data. Figure 1 is a schematic representation of our experimental apparatus. We decided to use Stroh's beer as the carbonated liquid because of the availability of physical constants that were needed in some of our computations about the motion of the bubbles.

The side projector was used as a light source to record the motion of the bubbles with the video camera. The video tape was replayed on a VCR with freeze frame and single frame advance features. Our camera recorded 30 frames per second, so the elapsed time for each frame was 1/30 sec. The meter stick was visible in our recorded frames,

---

William, who is known in the physics department as Andy, and Mark did this work as freshmen. Andy comes from Siloam, NC and intends to major in both Mathematics and Physics. Mark is a physics major from Greensboro , NC who is confined to a wheel chair.

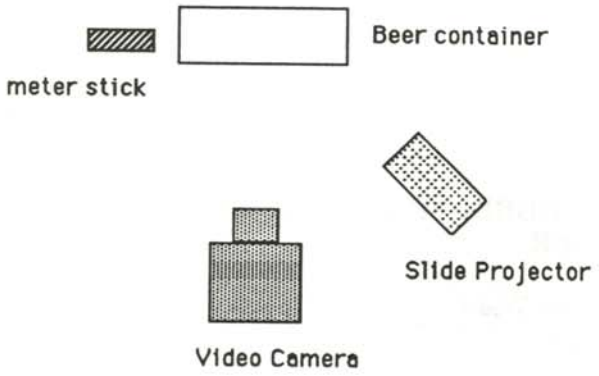

Figure 1
Schematic representation of experimental apparatus.

so we could obtain position measurements as a function of time. The speed of the bubbles was found using a least squares fit to the distance-time data.

EXPERIMENTAL RESULTS

We observed two different types of bubbles. A stream of tiny bubbles was present in the beer, but they were so small that we could not observe one individual bubble. The bubbles we used were large enough to be observed individually. All of the bubbles we used for data formed on the bottom of the container and floated up through the beer.

Figures 2-4 show plots of position vs time for these bubbles. The straight lines indicate that the bubbles rose with constant velocity. The average speed of the bubbles was $(1.5 \pm .1) \times 10^{-1}$ m/sec.

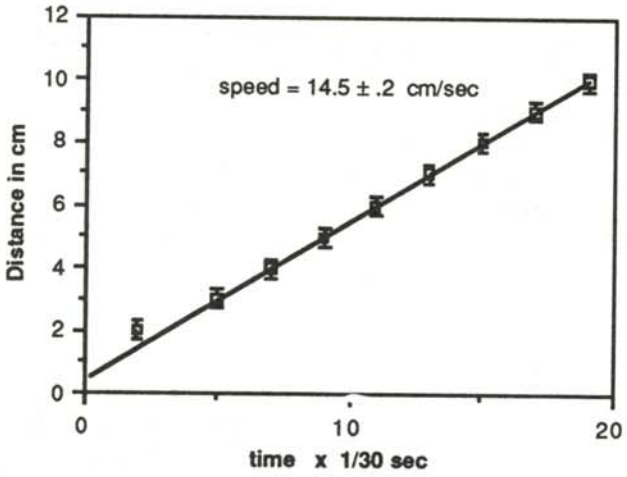

Figure 2
Distance-time graph for the first bubble.

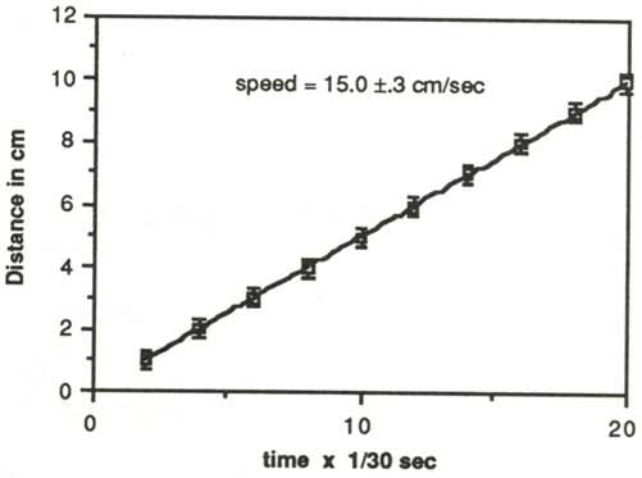

Figure 3
Distance time graph for bubble number 2.

COMPUTATIONAL ANALYSIS

This was not the kind of motion we expected. To understand what was happening, we decided to make a computational model of the motion. To do this, we created an acceleration function for the system. We then would use a computer simulation to determine positon vs time from this accleration and the initial velocity and position.

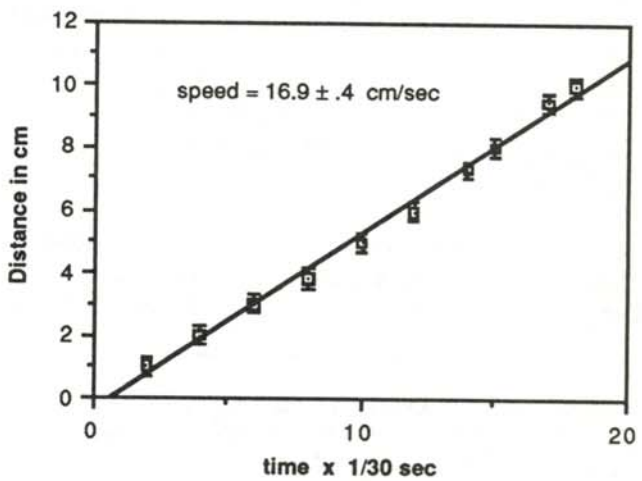

Figure 4
Distance-time graph for bubble number 3.

The forces acting on the bubble were gravity, bouyancy and friction. The gravitational force is:

$$F_g = - V \rho_o g \qquad (1)$$

where V is the volume of the bubble, ρ_o the density of the CO_2 gas in the bubble and g the acceleration due to gravity. The bouyant force is:

$$F_b = V \rho_f g \qquad (2)$$

where ρ_f is the density of the surrounding beer.

To determne which frictional drag law to use, we calculated the Reynold's number [2] for the motion of the bubbles in the beer. The Reynolds number is given by:

$$R = 2 \rho_f v r / \eta \qquad (3)$$

where v is the average velocty, r radius of the bubbles and η the viscosity of beer. The numerical values for the viscosity and density of the beer we used in the experiment were obtained from Stroh's Brewery [3].

The Reynold's number for the bubbles we measured was about 600. This means we could use a linear frictional drag law to model the motion:

$$F_f = - 6 \pi r \eta v \qquad (4)$$

where v is the velocity of the bubble.

The net force acting on the bubble is:

$$ma = - V \rho_o g + V \rho_f g - 6 \pi r \eta v. \qquad (5)$$

The mass of the bubble can be writen as $\rho_o V$.

Density of gas in bubble	1.98 kg/m^3
Density of beer	1.007 x 10^3 kg/m^3
Viscosity of beer	1.5 x 10-5 Pa sec

Table 1
Values of parameters used in simulation.

Substituting into Equation 5and solving for a gives:

$$a = g\left(\frac{\rho_f}{\rho_o} - 1\right) - \frac{9 \eta v}{2 r^2 \rho_o} \qquad (6)$$

Entering the values for the constants (shown in Table 1) into Equation 6 gives:

$$a = 4.97 \times 10^7 - (3.41 \times 10^{-5}) v / r^2 \qquad (7)$$

where a comes out in m/sec^2.

Equation 7 was used as the acceleration function for a Newton Half-step integration alogrithm for solving second order differential equations. [4]

The only free parameter in this simulation was the radius of the bubble. We made a number of runs of the computer simulation with different values of the radius. The motion of the bubbles was sharply determined by the size of the bubbles. Larger bubbles rose faster (as Aristotle predicted). We found that if we picked a radius of 3.3 x 10-5 meters, we got a bubble that rose at a constant speed of .15 m/sec. This set of conditions gave a good model for the real motion of the bubbles.

CONCLUSIONS

Our results are in conflict with other published works.[5] Our results show the bubbles moving at a constant speed and with constant radius rather than with increasing radius and hence increasing speed. For the bubble to move at constant speed, the radius must stay constant. The motion of the bubbles in the previous work was deduced from a single still photograph, showing bubbles with larger spacings as they rose. This effect is not necessarily in conflict with our results, if the rate at which bubbles are produced at a nucleation site depends upon time.

This, however, does not explain why we see bubbles whose size does not change as they rise up in the beer. As the bubbles rise, the process must not be a simple adiabatic or isothermal process. In both cases, the size of the bubbles would increase as they rose. Apparently there is some more complicated thermodynamic process taking place along

the interface between the bubble and the beer as the bubble rises.

ACKNOWLEDGMENTS

The authors would like to than Dr. Rexford Adelberger for his guidance and helpful discussions. The authors would also like to thank Mr. Carl Seibert of Stroh's Brewery for the discussions and for the physical constants of beer that he supplied.

REFERENCES

1) D.C. Giancoli, General Physics, Prentice-Hall Inc., Englewood Cliffs, 1984, pp. 390-401.

2) Ibid., pp 252-254.

3) Private communication, Carl Seibert, Stroh's Brewery, Corporate Headquarters, Detroit, MI.

4) We also checked these results with a 4th order Runge Kutta algorithm which converges more rapidly than the Newton Half-Step routine. Listings of both programs are available by writing to: Physics Department, Guilford College, Greensboro, NC, 27410.

5) C.F. Bophren, Clouds in a Glass of Beer - Simple Experiments in Atmospheric Physics, John Wiley and Sons, Inc., New York, 1987, p.5.

FACULTY SPONSOR

Dr. Rexford E. Adelberger
Physics Department
Guilford College
Greensboro, NC 27410